Available online at www.sciencedirect.com
SCIENCE DIRECT®
Journal of Power Sources 145 (2005) 30–39
JOURNAL OF POWER SOURCES
www.elsevier.com/locate/jpowsour

A high dynamic PEM fuel cell model with temperature effects☆

Yuyao Shan*, Song-Yul Choe

Department of Mechanical Engineering, Auburn University, Auburn, 36830 AL, USA

Received 26 November 2004; accepted 23 December 2004
Available online 20 March 2005

Abstract

Safe and reliable operation of a fuel cell requires proper management of the water and heat that are produced as by-products. Most of the current models for the cell used for an analysis of the fuel cell system are based on the empirical polarization curve and neglect the dynamic effects of water concentration, temperature and reactant distribution on the characteristics. The new model proposed in this paper is constructed upon the layers of a cell, taking into account the following factors: (1) dynamics in temperature gradient across the fuel cell; (2) dynamics in water concentration redistribution in the membrane; (3) dynamics in proton concentration in the cathode catalyst layer; (4) dynamics in reactant concentration redistribution in the cathode GDL. Simulations have been performed to analyze the effects of load currents on the behaviors of the fuel cell. In the future, the fuel cell model will be extended to a stack model and integrated with system models. All of the models will be implemented on a real time system that optimizes the computation time by a parallelization of solvers, which provides an environment to analyze the performance and optimize design parameters of the PEM fuel cell system and components.
© 2005 Published by Elsevier B.V.

Keywords: PEMFC; Dynamic; Temperature; Water; Efficiency; Startup

1. Introduction

The PEM fuel cell is a strong candidate for use as an alternative power source in future vehicle and power conditioning applications. The effects of electric loads on temperature, water in the stack and reactants are crucial issues that must be considered for the optimum design of fuel cell powered systems. Currently, fuel cell stack models are being employed to analyze these effects. However, the simulation results do not incorporate either the dynamic or transient aspects of the fuel cell system in operating environments.

As a matter of fact, the dynamic power output and efficiency profile of a PEMFC is strongly influenced by the variation of the temperature, reactant and product transfer in the fuel cell caused by a current load.

Firstly, the temperature significantly affects the performance of a fuel cell by influencing the water removal and reactants activity, etc. A current proposed model assumes a constant working temperature [1], which does not incorporate the reality that this working temperature dynamically varies at different load currents, as well as during startup and shut-down of the fuel cell system. Some authors proposed improved models, with Amphlett et al. [2] using the first empirical thermal model, and Gurski et al. [3] considering the reactant flows and coolant control based upon the previous model. Others proposed models calculating the temperature variation of the stack, cell [4–10] or two electrodes and MEA [11,12]. B. Wetton et al. [13] proposed an explicit thermal model to analyze the temperature gradient of different layers in the fuel cell stack considering the stack asymmetric effects, which does not include dynamics. Recently, M. Sundaresan published the most detailed 1D thermal dynamic model [14]. However, the flow of species at the inlet must be the same as that at the outlet. Thus, no fluid dynamics is considered in the model.

Secondly, the proton transport in the membrane and its associated ohmic losses mainly determine the characteristics

☆ This paper was presented at the 2004 Fuel Cell Seminar, San Antonio, TX, USA.

* Corresponding author. Tel.: +1 334 220 6533.
E-mail addresses: shanyuy@auburn.edu (Y. Shan), choe@eng.auburn.edu (S.-Y. Choe).

0378-7753/$ – see front matter © 2005 Published by Elsevier B.V.
doi:10.1016/j.jpowsour.2004.12.033

Nomenclature

Alphabets

a	species activity
A	area (m^2)
C	mass concentration ($kg\,m^{-3}$)
D	diffusion coefficient ($m^2\,s^{-1}$)
F	faraday number
G	gibbs free energy ($J\,mol^{-1}$)
H	enthalpy ($J\,mol^{-1}$)
i	current density ($A\,m^{-2}$)
j	exchange current density ($A\,m^{-2}$)
l	thickness (m)
m	mass (kg)
M	mole mass ($kg\,mol^{-1}$)
n_d	electro-osmotic drag coefficient
N	mole flux ($mol\,s^{-1}\,m^{-2}$)
P	pressure (partial pressure) (Pa)
R	universal gas constant
R_{mem}	proton transfer resistance (Ω)
R_{ab}	electrical resistance (Ω)
S	entropy ($J\,mol^{-1}\,K^{-1}$)
T	temperature (K)
W	mass flux ($kg\,s^{-1}\,m^{-2}$)

Greek symbols

ε	porosity
λ	water uptake coefficient
ρ	density ($kg\,m^{-3}$)
τ	tortuosity

Superscripts and subscripts

an	anode
ca	cathode
cv	control volume
d	gas diffusion layer
g	gas
i	index
l	liquid
mem	membrane layer
ref	reference value
sat	saturation
sou	source

of ohmic polarization. The proton conductivity has been regarded as constant, temperature dependent [1] or temperature and water concentration dependent variables [15]. Recently, Pukrushpan et al. [16] proposed the most comprehensive model that considers the dependence of the proton conductivity on the water concentration and temperature. However, the water concentration of the membrane is obtained from the membrane relative humidity (RH) on an average of the anode and cathode RH. In fact, the RH in the anode and cathode varies rapidly, while the RH in the membrane does slowly because the amount of water residing in both sides is relatively less than in the membrane [15].

Thirdly, the oxygen concentration in the GDL on the cathode side is continuously changing in operating environments and significantly affects the performance of the cell. Therefore, plenty of models considering multi-phase multi-species have been employed to investigate the transport phenomena in the GDL. However, those models do not consider the dynamics. Recently, Pukrushpan et al. proposed a dynamic model with lumped parameters to predict the gas dynamics in a cathode electrode, which does not consider the effects in the GDL [16]. In this paper, we use a 1D single-phase model to represent the dynamics present in the GDL.

2. Model setup and assumptions

The model has been developed on the basis of layers in a cell that consist of a MEA, two gas diffusion layers and two gas channels sandwiched by two coolant channels, as shown in Fig. 1. The input variables for the model are current load, mass flow rate, the gas components fraction, temperature, pressure and relative humidity of reactants as well as the temperature and velocity of coolants at the inlets.

The main assumptions made for the new model are as follows:

1. Reactants are ideal gases.
2. There is no pressure gradient between the anode and cathode side; it means no convection but only diffusion for gas transport is considered.
3. There is no gas pressure drop from the inlet to the outlet of the gas channel.
4. The temperature gradient is linear across the layers in a fuel cell.
5. The thermal conductivity for the materials in a fuel cell is constant.
6. There is no contact resistance.
7. Anodic over-potential is negligible.

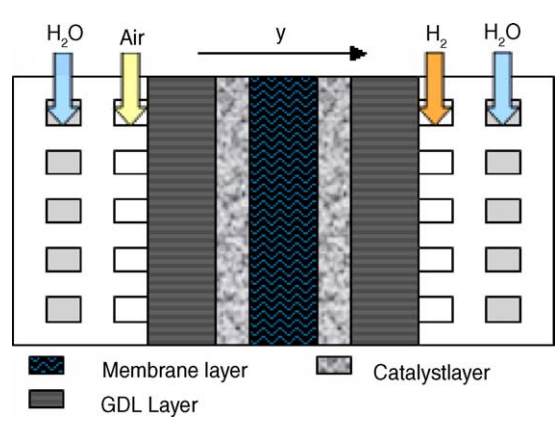

Fig. 1. Schematic simulation domain.

8. There is no current density gradient across the cathode catalyst layer; it means that the reactants completely reacted as soon as it reaches to the cathode catalyst layer surface.
9. Based on these assumptions, five sub-models have been developed and are described in the following sections.

3. Model description

3.1. Electrochemical model

Generally, the overall chemical reaction of the PEM fuel cell can be described by using the following expressions, illustrating that a chemical reaction of hydrogen and oxygen molecules produces electricity, water and heat as a by-product:

$$H_2 + \tfrac{1}{2}O_2 \rightarrow H_2O + Q_{res} + V_{cell}$$

The output cell voltage V_{cell} is the difference between the open circuit voltage (OCV) E_0 and over-potentials η and V_{ohm}.

$$V_{cell} = E_0 - \eta - V_{ohm} \tag{1}$$

By neglecting the dependence of the OCV on the reactant pressure, the relationship between the OCV and the temperature can be simplified with the empirical parameter dE_0/dT. If the reactant is ideal, its activity can be described by using Eq. (2), where index i indicates H_2 and O_2, while P_i is the partial pressure of gas components, and P_0 is the overall pressure of both the anode and cathode side. Then, E_0 can be derived by modifying the Nernst Eq. (3).

$$a_i = \frac{P_i}{P_0} \tag{2}$$

$$E_0 = E_{ref} + \frac{dE_0}{dT}(T - T_{ref}) + \frac{RT}{2F}\ln(a_{H_2}^{1} a_{O_2}^{0.5}) \tag{3}$$

The anodic over-potential is negligible; while the η represents the over-potential of the cathode catalyst layer. Under the further assumptions that the asymmetric parameter of the reaction is (1) and (8), the Butler–Volmer equation leads to Eq. (4) that describes the over-potential on the cathode side.

$$i = j_0 \frac{A_{cata,eff}}{A_{cell}} \left\{ \frac{p_{O_2}}{p_{O_2,ref}} \frac{[H^+]}{[H^+]_{ref}} \exp\left(\frac{F\eta}{RT}\right) - 1 \right\} \tag{4}$$

The ohmic over-potential V_{ohm} is determined by the product of the current density and the proton resistance R_{mem} according to Ohm's law (5).

$$V_{ohm} = iR_{mem} \tag{5}$$

3.2. Thermal model for a cell

If a cell is assembled with cubic layers whose thermophysical properties are isotropic and constant, and then according to the energy conservation equation, the total energy changes in a controlled volume equals the sum of the energy exchange at boundaries and internal energy resources. In fact, the energy exchanges at boundaries occur by three factors: (a) the mass flow into each volume; (b) the conduction heat transfer across the cell; (c) the convection heat transfer occurring between bipolar plates with the coolant and the reactants. Thus, the thermal dynamic behavior can be described with the following energy conservation equation:

$$\sum_i Cp_i C_{i,mass} A_{cell} l_{cv} \frac{dT_{cv}}{dt} = \underbrace{\sum \dot{m}_{in} A_{cell} Cp_j (T_{in} - T_{cv})}_{\text{mass flow in}} + \underbrace{\dot{Q}_{Conv} A_{cell}}_{\text{convection heat transfer}} + \underbrace{\dot{Q}_{Cond} A_{cell}}_{\text{conduction heat transfer}} + \underbrace{\dot{Q}_{sou}}_{\text{sources}} \tag{6}$$

On the other hand, the internal energy source is composed of the entropy loss and the chemical energy required for protons to overcome the barrier of the over-potentials in both catalyst layers (Eq. (7)). In addition, other heat sources are ohmic losses caused by a transport of electrons and protons in the cell:

$$\dot{Q}_{sou} = iA_{cell}\left(-\frac{T\Delta S}{4F} + \eta + iA_{cell}R_{ele}\right) \tag{7}$$

In fact, the change of entropy due to the electrochemical reaction (Eqs. (8) and (9)) in both of the catalysts sides predominantly influences the energy sources term according to the calculation shown below.

$$H_2 \rightleftharpoons 2H^+_{(aq)} + 2e_{(pt)}^- \tag{8}$$

$$O_2 + 2H^+ + 2e^- \rightleftharpoons H_2O_{(l)} \tag{9}$$

In order to obtain the entropy change of these reactions, the zero point of semi-absolute entropy is taken as a reference according to [17]:

$$s[H^+_{(aq)}] \equiv 0 \tag{10}$$

The entropy of an electron obtained from the standard hydrogen electrode results in the following equations [17]:

$$\Delta S_{SHE} = \frac{\Delta H_{SHE} - \Delta G_{SHE}}{T} = 0 \tag{11}$$

$$s[e_{(pt)}^-] = \frac{1}{2}s[H_2] = 65.29\,\mathrm{J\,mol^{-1}\,K^{-1}} \tag{12}$$

Therefore, the entropy change of the cathode reaction is equal to the sum of that in water, oxygen and electron:

$$\Delta S_{ca} = s[H_2O_{(l)}] - \frac{1}{2}s[O_2] - 2s[e_{(pt)}^-] = 69.91 - \frac{1}{2} \times 205.03 - 2 \times 65.29 = -163\,\mathrm{J\,mol^{-1}\,K^{-1}} \tag{13}$$

If the anode is assumed as a standard electrode, the anodic entropy change becomes 0.

3.3. Proton conducting model for membrane

The membrane resistance is a function of the temperature and water content in a membrane layer, which is described as follows [16]:

$$R_{\text{mem}} = \frac{l_{\text{mem}}}{(b_{11}\lambda_{\text{mem}} - b_{12})\exp\left(b_2\left(\frac{1}{303} - \frac{1}{T_{\text{mem}}}\right)\right)} \tag{14}$$

where the temperature T_{mem} can be derived from the previous Eq. (6), while the membrane water content λ_{mem} can be described by using the water mass concentration [15] and the mass conservation equation [16]:

$$\lambda_{\text{mem}} = \frac{C_{\text{H}_2\text{O,mass}}/M_{\text{H}_2\text{O}}}{\rho_{\text{dry,mem}}/M_{\text{mem}} - bC_{\text{H}_2\text{O,mass}}/M_{\text{H}_2\text{O}}} \tag{15}$$

$$\frac{\text{d}m_{\text{water}}}{\text{d}t} = \frac{\text{d}(C_{\text{H}_2\text{O,mass}}A_{\text{cell}}l_{\text{mem}})}{\text{d}t} = \begin{pmatrix} W_{\text{ele,mem,an}} - W_{\text{ele,mem,ca}} + \\ W_{\text{diff,mem,ca}} + W_{\text{diff,mem,an}} \end{pmatrix} \tag{16}$$

The electro-osmotic driving force created by the different electrochemical potential at the anode and cathode determines the water mass flows of $W_{\text{ele,mem,an}}$ and $W_{\text{ele,mem,ca}}$ at the boundaries of the membrane layer. In addition, the diffusion caused by the water concentration gradient at the two boundaries makes up the mass flows of $W_{\text{diff,mem,an}}$ and $W_{\text{diff,mem,ca}}$. Those relationships are described by Eqs. (17)–(19), proposed by Spriger [24].

$$n_{\text{d}} = 0.0029\lambda_{\text{mem}}^2 + 0.05\lambda_{\text{mem}} - 3.4 \times 10^{-19} \tag{17}$$

$$W_{\text{ele,mem},i} = M_{\text{water}}A_{\text{cell}}n_{\text{d},i}\frac{i}{F} \tag{18}$$

$$W_{\text{diff,mem},i} = M_{\text{water}}A_{\text{cell}}D_{\text{water}}\frac{C_i - C_{\text{mid}}}{l_{\text{mem}}} \tag{19}$$

Hence, the diffusion coefficient D_{water} and the water concentration C_i are calculated from the empirical Eq. [24] expressed as a function of membrane water content λ_{mem}:

$$D_{\text{water}} = D(\lambda_{\text{mem}})\exp\left(2416\left(\frac{1}{303} - \frac{1}{T_{\text{mem}}}\right)\right) \tag{20}$$

$$D(\lambda_{\text{mem}}) = \begin{cases} 10^{-6} & 2 > \lambda_{\text{mem}} \\ 10^{-6}(1 + 2(\lambda_{\text{mem}} - 3)) & 3 \geq \lambda_{\text{mem}} \geq 2 \\ 10^{-6}(3 - 1.67(\lambda_{\text{mem}} - 3)) & 4.5 > \lambda_{\text{mem}} > 3 \\ 1.25 \times 10^{-6} & \lambda_{\text{mem}} \geq 4.5 \end{cases} \tag{21}$$

The boundary water content λ_i is a function of water activity a_i, which is calculated from the water vapor partial pressure:

$$\lambda_i = \begin{cases} 0.043 + 17.81a_i - 39.85a_i^2 + 36a_i^3 & 1 \geq a_i > 0 \\ 14 + 1.4(a_i - 1) & 3 \geq a_i > 1 \\ 16.8 & 3 \leq a_i \end{cases} \tag{22}$$

$$a_i = \frac{P_{v,i}}{P_{\text{sat},i}} \tag{23}$$

3.4. Proton dynamic model in the cathode catalyst layer

The dynamic behavior of a fuel cell at a load is investigated by experiments. When the output current changes abruptly, the output voltage of the fuel cell reacts with an overshoot [18]. These dynamics result from different physical phenomena of reactants and their chemical reaction in the cell, such as dynamics filling in the gas flow channel, diffusing reactants through the GDL and reacting process in the double layer at the interface of electrodes. Ceraolo et al. explained the dynamic effects with a relationship between the number of mobile protons and water content [1]. As a matter of fact, when the current density increases, the hydration of the polymeric electrolyte near the cathode catalyst tends to rise as well; consequently, the proton concentration near the cathode catalyst increases rapidly. On the other hand, the proton concentration will decrease slowly at a decrease of current. Thus, the dynamics can be described by the following differential equation using the proton concentration as a variable [1]:

$$\delta\left(-\frac{\partial\dot{C}_{\text{H}^+}}{\partial t}\right)\frac{\partial\dot{C}_{\text{H}^+}}{\partial t} + \frac{\dot{C}_{\text{H}^+}}{\tau_{\text{H}^+}} = \frac{1 + \alpha_{\text{H}^+}i^3}{\tau_{\text{H}^+}} \tag{24}$$

$\dot{C}_{\text{H}^+} = [\text{H}^+]/[\text{H}^+]_{\text{ref}}$ is the dimensionless proton concentration, $\delta(\,)$ the Heaviside function, and τ_{H^+} and α_{H^+} are empirical parameters.

Fig. 2 shows the calculated response. The voltage decreases quickly when the current density increases. However,

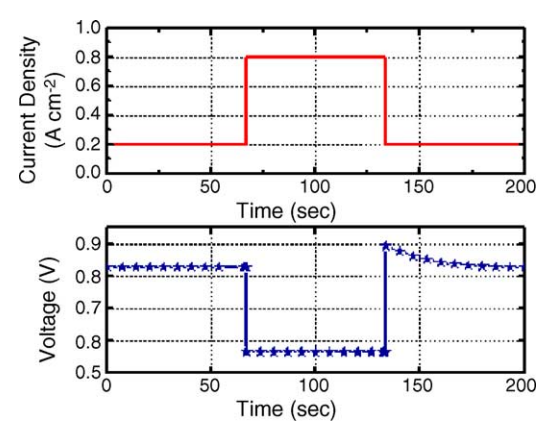

Fig. 2. Voltage response by a consideration of proton concentration.

the voltage first reaches its highest value and then damps with a time constant that is associated with the proton concentration, as the current density decreases.

3.5. GDL reactant model for cathode

Air contains not only oxygen but also nitrogen and water vapor. The air entering the cell diffuses through the GDL before reaching the catalyst layer. The diffusion effect is described by using the mass conservation (25) and Stefan–Maxwell equations (26):

$$\frac{\varepsilon_g}{RT}\frac{\partial P_i}{\partial t} + \frac{\partial N_i}{\partial y} = 0 \tag{25}$$

$$\frac{\varepsilon_g}{\tau^2}\frac{\partial P_i}{\partial y} = \sum_{k=1}^{3}\frac{RT}{P_{ca}D_{ik}}(P_iN_k - P_kN_i) \tag{26}$$

Hence, $i, k \in (1, 3)$, where P_1 is the oxygen partial pressure, and $P_2 = P_{sat}(T)$ and P_3 are the water vapor and the nitrogen partial pressure, respectively. The diffusion coefficient $P_{ca}D_{ik} = D_{ik,eff} = D_{ik,eff}(T)$, and the cathode pressure of P_{ca} is the summation of the species partial pressures. The parameter τ is a constant describing the pore curvature of the GDL.

The partial differential equation (PDE) systems above can further be simplified by using the following PDE [1], whereby ξ is the dimensionless distance y/l_d:

$$\frac{\partial P_{O_2}}{\partial t} = \omega\frac{\partial^2 P_{O_2}}{\partial \xi^2} - \psi\frac{i}{4F}\frac{\partial P_{O_2}}{\partial \xi} \tag{27}$$

$$\omega = \frac{1}{\tau^2 l_d^2((P_{sat}/D_{12}) + (P_{ca} - P_{sat})/D_{12})} \tag{28}$$

$$\psi = \frac{RT}{\varepsilon_g l_d(P_{ca} - P_{sat})} \tag{29}$$

In order to investigate the effects of the GDL on dynamics, simulations have been run to analyze the relationship between the GDL thickness and the dynamics of oxygen by diffusions. Fig. 3 shows the dynamic response of the oxygen partial pressure at the interface of the cathode GDL and cathode catalyst layer. The results show that the oxygen partial pressure drops rapidly when a step current (Fig. 4) is applied. Thus, the concentration over-potential increases. Accordingly, the thickness of the GDL is one of the factors influencing the dynamic response. Moreover, the steady state is reached by the thin GDL more quickly than by the thick one.

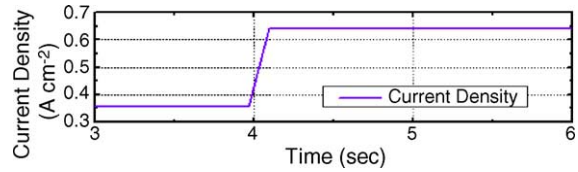

Fig. 4. Current input.

Further analysis has been undertaken to discover how the reactant partial pressure is distributed along the GDL by the given pressure (Fig. 5) and current step. Fig. 6 shows the cathode oxygen partial pressures and their responses depending upon the thickness ratio. The analysis shows that the dynamic response of the oxygen partial pressure is highly dependent upon the geometrical locations. When the cathode inlet pressure changes, the pressure at the catalysts side responds with a time delay before it has reached the steady state, which is caused by the diffusion of the reactant. Accordingly, the over-potential cannot be manipulated instantly.

The dynamic responses of the oxygen concentration at the catalyst layer are illustrated in Fig. 7. The oxygen concentration is strongly influenced by the thickness of the GDL. The thinner the layer becomes, the shorter the response time gets. On the other hand, when the inlet pressure increases (Fig. 5), the partial pressure at the catalysts tends to follow its increase, but the amounts of the recovered partial pressure compared to Fig. 3 depend on the thickness. Therefore, the settle times to the steady state become constant regardless of the thickness of the GDL.

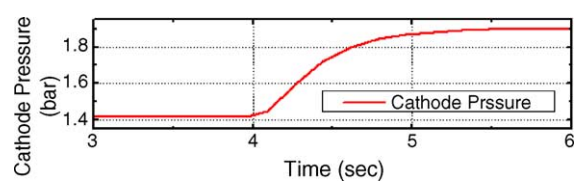

Fig. 5. Dynamic cathode pressure input.

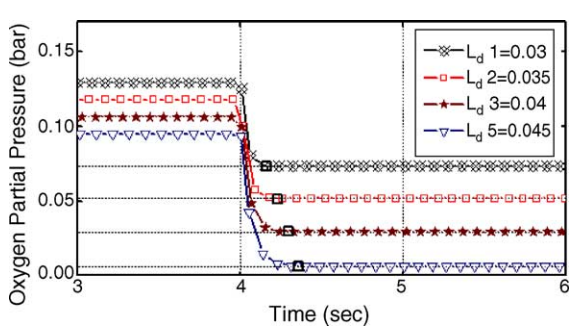

Fig. 3. Oxygen concentration response dependent upon GDL thickness at $P = 1$ bar and $T = 353\,^{\circ}$K.

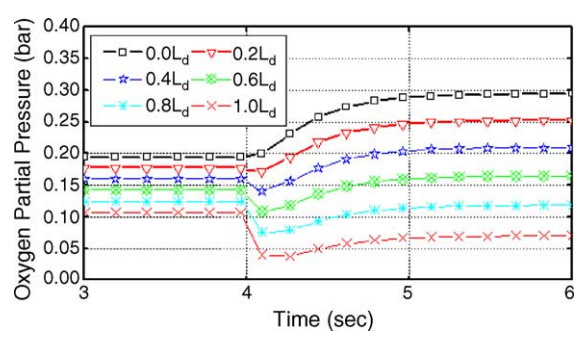

Fig. 6. Oxygen concentration response to the dynamic current input and cathode pressure at different depths.

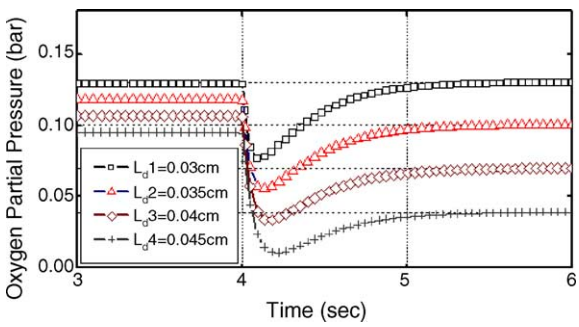

Fig. 7. Oxygen concentration dynamic response for different GDL thicknesses.

In this part, the effects of material properties on the dynamics are analyzed by a given current step. Figs. 8 and 9 show the dependences on porosity and tortuosity. Generally, the GDL with a high porosity allows less pressure drops than that with the lower one. However, the GDL with a high tortuosity causes higher pressure drops than the low one because of a long path for the oxygen transported. When a step current is applied to the cell, the oxygen consumption on the catalysts side will be increasing. Instantly, the high porosity enables more oxygen to transfer from the inlet to the catalysts side, and, subsequently, the oxygen partial pressure at the catalysts can quickly follows the pressure changes at the inlet. Thus, the GDL with a high porosity dynamically responds to the pressure increase. When the tortuosity increases, the dynamic response time slows from the same effects as prolonged geometry and the associated pressure drop. The settle times remain unchanged, as in the analysis for different thickness.

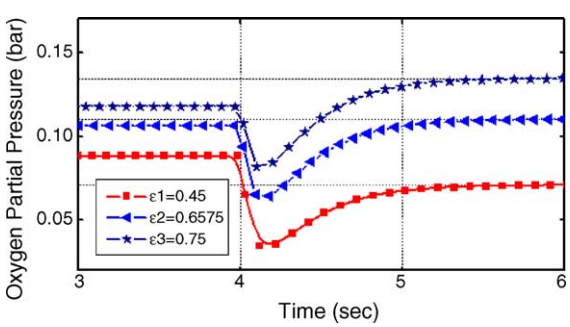

Fig. 8. Dynamic response of oxygen concentration for different porosities.

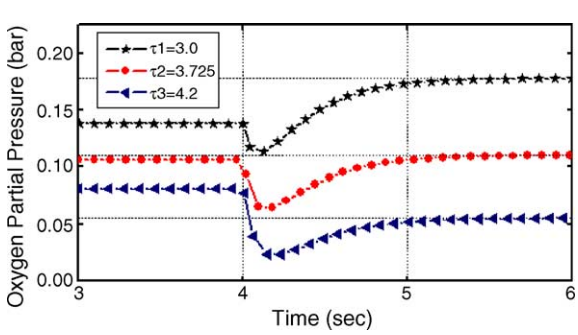

Fig. 9. Dynamic response of oxygen concentration for different tortuosities.

4. Simulation results

All of the aforementioned models are coded with MATLAB and C. Multi-run simulations have been conducted to investigate the static and dynamic behavior of a single cell. The static behavior is analyzed by calculating the typical polarization, which takes into account variables such as, working temperature, pressure, stoichimetric number and relative humidity (RH) at the cathode inlet. The dynamic characteristic considers two aspects, the startup and the transient response on the current as a step load.

4.1. Parameters and reference data

The parameters and reference data for the models chosen are as follows (see Table 1), and they are partially empirical [1,16,21].

4.2. Static behavior

Fig. 10 shows the temperature dependent *I–V* characteristics from 333 to 363 K with a step of 10 K. As the temperature increases, the water removal will be more eased. The effects are considerably high at the range of the higher cell current, where more water is produced. This result is comparable with the CFD analysis [19].

Fig. 11 shows the pressure dependent polarization curve. As the pressure increases, the oxygen concentration at the surface of the catalysts layer tends to increase, too. Thus, the concentration over-potential gets lower. Otherwise, the over-potential becomes higher because of the oxygen starvation.

Table 1
Empirical/reference parameters

Electronic reactions model	
P_0	1.0 bar
T_{ref}	343.15 K
E_{ref}	0.975 V [1]
dE_0/dT	0.00027 V K^{-1} [1]
$A_{cata,eff}/A_{cell}$	$f(I, T, P_{O_2})$ [1]
Gas transport model	
D_{eff}	$f(P, T)$ m^2 s^{-1} [1]
P_{sat}	$f(T)$ bar [1]
Thermal model	
H_{gas}	$f(P, T)$ [21]
C_{p-gas}	$f(P, T)$ [21]
P_{gas}	$f(P, T)$ [21]
Proton conducting model	
b_{11}	0.5139 [16]
b_{12}	0.326 [16]
b_2	350 [16]
b	0.0126 [16]
n_d	$f(C_{water})$ [16]
D_w	$f(T, C_{water})$ [16]
Proton concentration model	
α_{H^+}	5.87E–12 $(m^2 A^{-1})^3$ [1]
τ_{H^+}	12.78 s [1]

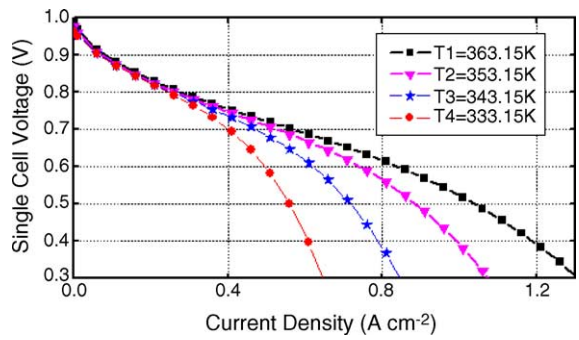

Fig. 10. *I–V* curve for different cell working temperature. Cell: $P = 1.0$ bar.

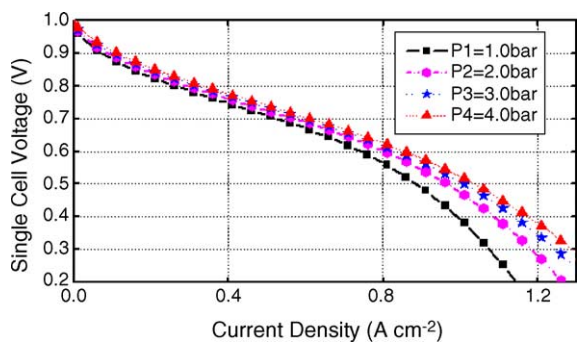

Fig. 11. *I–V* curve for different cell gas pressure. Cell: $T = 353.15$ K.

The results are also comparable with the CFD analysis [19].

Fig. 12 shows the stoichimetric number dependent *I–V* curve at a constant temperature and pressure. When the stoichimetric number is low, the removal of water at the cathode outlet flow decreases. Thus, the water concentration in the membrane layer increases. Consequently, the membrane resistance and the resulting ohmic over-potential become lower. However, the low stoichimetric number adversely affects the cathode over-potential at the high current because of the excessive water in the catalysts.

Fig. 13 shows the output voltage of a cell influenced by relative humidity at the cathode inlet. When the humidity increases at the cathode side, the air transported to the catalysts

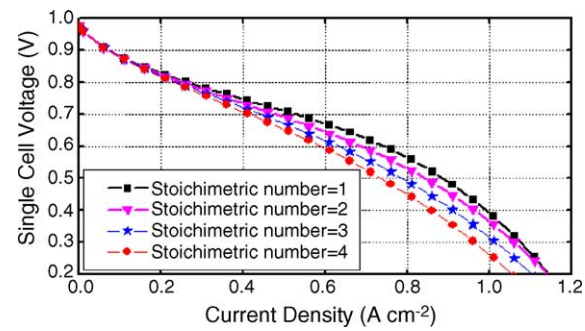

Fig. 12. *I–V* curve for different stoichimetric number. Cell: $T = 353.15$ K, $P = 1.0$ bar.

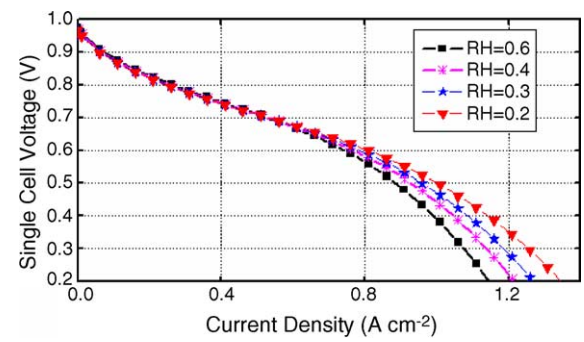

Fig. 13. *I–V* curve for different RH at the cathode inlet. Cell: $T = 353.15$ K, $P = 1.0$ bar.

will be blocked, and the cathode over-potential will increase, especially at the high current range. The results are comparable to the experimental data [20].

4.3. Dynamic behaviors

For a startup of dynamic simulations, initial values are necessary for variables such as layer temperature, membrane water concentration, GDL air and oxygen concentration and gas channel pressure. Fig. 14 shows the setup for the simulation of a single cell from layer 1 to 11.

Geometrical and thermo-physical data for the layers are summarized in Table 2.

Table 2
Simulation data

	Thickness (m)	Heat conductivity ($Wm^{-1}\,k^{-1}$)	Heat capacity ($J\,Kg^{-1}\,K^{-1}$)	Density ($Kg\,m^{-3}$)
GDL	0.0004	65	840	2000
Catalyst layer	0.000065	0.2	770	387
Membrane layer	0.000183	0.21	1100	1967
Gas channel	0.001	52	935	1400
Plate	0.001	52	935	1400
Coolant channel	0.001	30	935	1400

GDL porosity	0.5
GDL tortuosity	3.725
Bipolar plate contact area percentage	0.55
Membrane molecular mass	$1.1\,Kg\,mol^{-1}$
Fuel cell area	$0.0367\,m^2$
Fuel cell active area	$0.03\,m^2$

Fig. 14. Simulation setup.

4.3.1. Startup

The startup temperature for the cell model is initially set to 298.15 K. The value of current density is increased continuously for the first 350 s in order to quickly raise the temperature to 353.15 K, which is assumed as a typical working temperature. In addition, a temperature controller is built in the simulation, as if a coolant subsystem turned on and off at this set point to extract the excessive heat produced in the cell. Fig. 15 shows the dynamic behavior of the temperature for different layers and voltage, as well as the efficiency during a startup. It took 8 min for the cell to reach to the working temperature (Fig. 15a). Generally, the temperature profiles in each of the layers tend to follow the current waveform, because of the associated energy losses occurring in the layers. Particularly, the temperature in the membrane and catalysts layer is the highest, which results from ohmic losses due to the membrane resistance and the heat released by the chemical reaction. The average difference of temperature between these two layers and other layers on the anode and cathode side amounts to 3 and 2 K, respectively. Corresponding voltage and power are shown in Fig. 15c. When the current increases, the over-potentials increase, and, subsequently, the voltage and power decrease. While the temperature is rising, the voltage fluctuates slightly during the startup. When the current had been kept constant after the 350 s, the amount of water generated in the catalyst layer becomes constant. On the other hand, the continuously increased temperature leads to a high saturation pressure in the cell, which enables water residing in the catalysts to be quickly removed [23]. Otherwise, water would be flooding and blocking further influx of the oxygen into the catalysts. Therefore, the cell voltage increases rapidly. Thereafter, the water concentration in the membrane continuously decreases by the electro-osmotic force and diffusion effects, and the corresponding proton conductivity will be decreased. Thus, the cell voltage slightly drops after the temperature has reached a steady state. The overall efficiency of a cell is also strongly influenced by the variation of temperature (Fig. 15d).

Fig. 16 shows the dynamic behavior of the temperature distribution across the fuel cell at 50 s and 7 min during a startup process. The catalyst on the cathode side shows the highest peak because of the losses associated with the overpotential being higher than on the anode side. For the first 30 s, the temperature rises slowly because of the slow slope of the current. The maximum difference of temperature between the GDL at the anode side and the membrane has been shown to reach 1 K. The higher the current is, the more heat is generated. Thus, the rise of temperature in the layers is accelerated. When the startup is ended after 7 min, the temperature in the catalyst rises up to 353 K, approximately 2 K higher than the anode side catalyst. Then, the peak point of the temperature

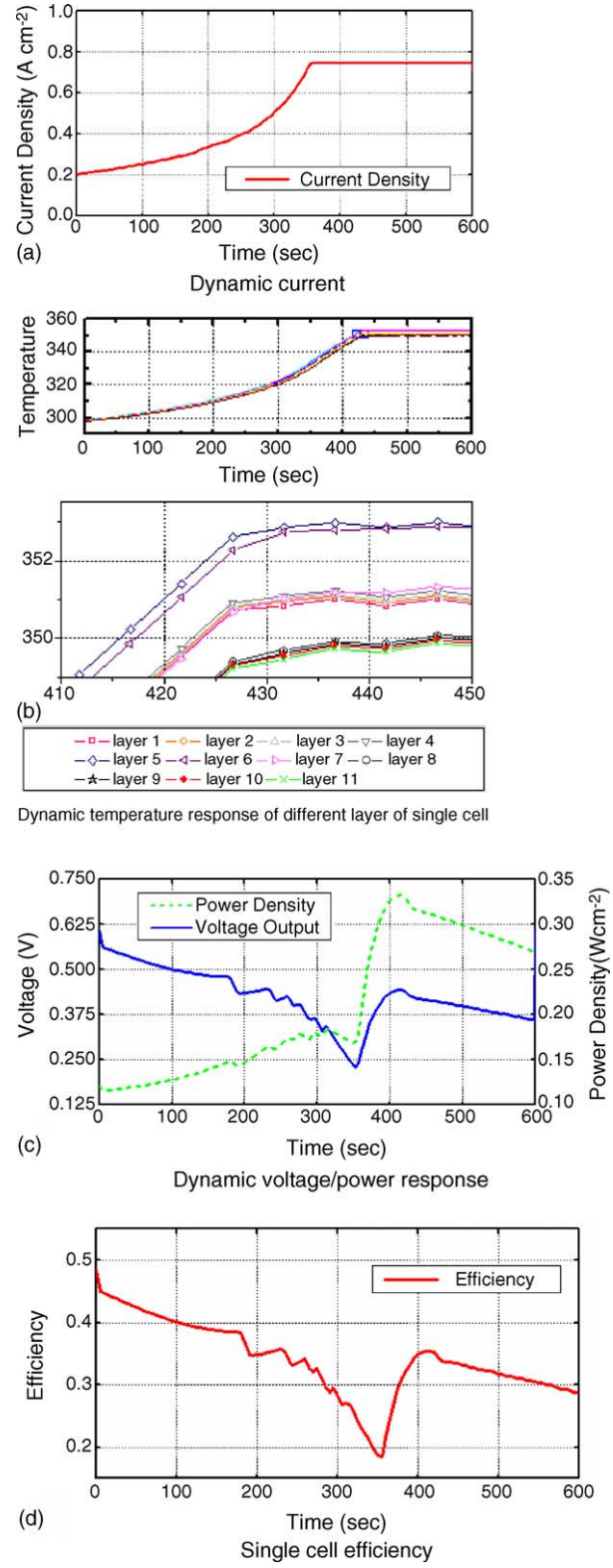

Fig. 15. Simulation results.

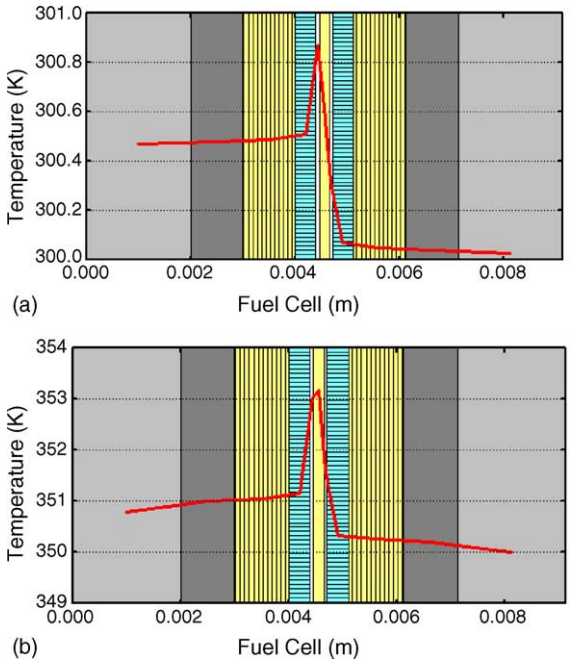

Fig. 16. Temperature gradient across the cell (left to right: cathode coolant channel to anode coolant channel): (a) 50 s and (b) 7 min after startup.

is moved from the catalyst to the membrane, which results from the dehydration of the membrane and the associated increase of losses. The dehydration is mainly caused by diffusions of water from the membrane to both sides because of higher water concentration in the membrane than in the gas channel sides. On the other hand, the increased number of protons transported takes up more water from the membrane to the cathode. Consequently, the resistance in the membrane is increased and shows the highest temperature among the layers.

4.3.2. Transient response

In order to analyze the dynamic response on a power demand, a step current with 0.8–0.4 A cm^{-2} at the 600 s is applied. Fig. 17 shows the response of the temperature in the different layers (b), voltage (c), power output (c) and efficiency (d).

The operating temperature is automatically controlled by the coolant system, the reference value for which is set to 353.15 K. The on–off control of the coolants causes a slight fluctuation of the temperature waveforms until 600 s. When the current suddenly decreases, the heat generated at the cathode catalyst and membrane layer decreases rapidly and leads to a temperature drop at these two layers. Then, the coolant system is turned off. The heat is transferred by the temperature gradient from the layers into the bipolar plates and stored there. Thus, the temperature of both bipolar plates tends to increase, and the temperature gradient begins to decrease. As a result, the amount of heat removed from the catalyst and membrane layers is again decreased.

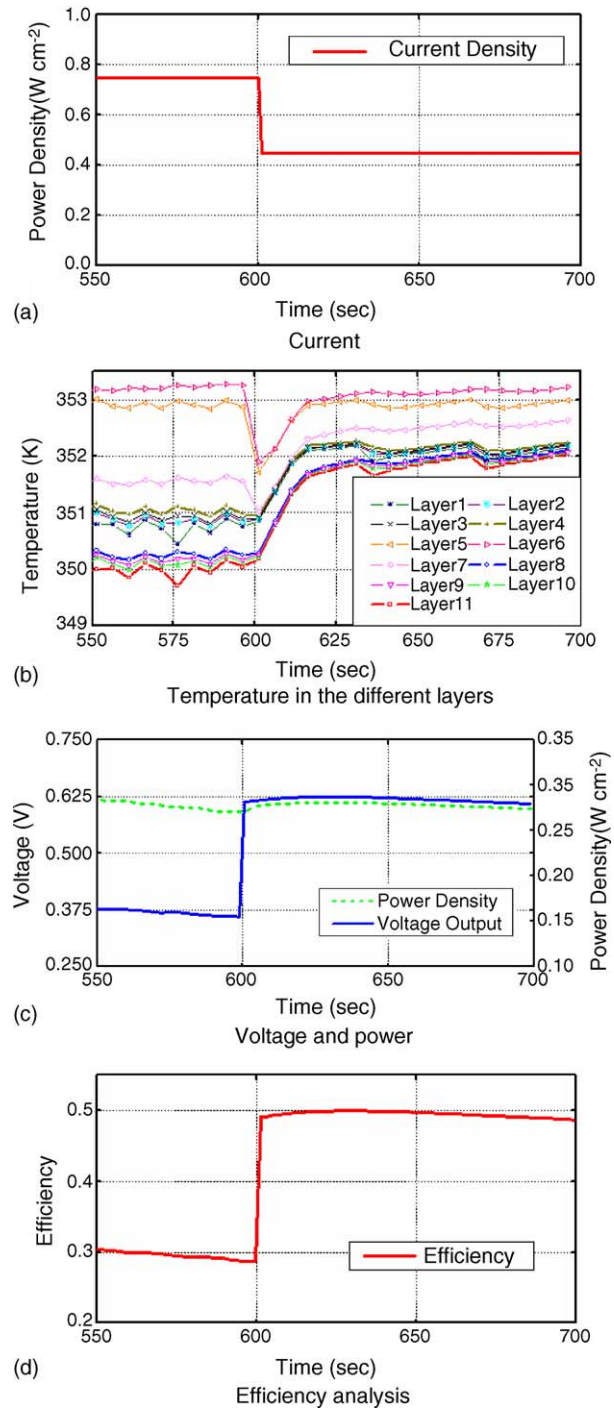

Fig. 17. Analysis of transient behavior of temperature, voltage, power and efficiency upon a current step.

When the temperature of the catalyst and the membrane layer reaches its lowest point, the temperature of all the layers will rise again due to the accumulated heat after the coolant is turned off. Finally, it reaches the steady state after around 10 s.

The effects of the temperature variation on the output voltage are slightly different from the temperature profiles.

When the current decreases, the voltage rapidly increases and shows a slight overshoot. Then, the voltage slowly elevates and drops back to a steady state. The first overshoot of the voltage results from the variation of the proton concentration in the cathode catalyst layer, while the first half of the voltage arc is caused by the temperature increase in all the layers, and the rest by the decrease of water concentration in the membrane layer. The efficiency profile is the same as the behaviors of the output voltage, but the power remains almost the same as before the current was applied. The voltage response is comparable to an experimental result [22].

5. Conclusion

In this paper, a new dynamic model for the PEM fuel cell is proposed to predict responses of the electric load on the cell. Emphasis is placed on the temperature response to the dynamic load. The model is constructed with layers that include membrane, catalysts, gas diffusion layers and bipolar plates. The models for the layers are separately and mathematically described. The analyses delivered surprising results in the effects of electric loads on temperature, voltage and efficiency. Particularly, description of interrelated physical variables by varying temperature provides a more realistic tool that can be utilized for deriving design parameters of a fuel cell stack and systems. As an example, a startup process and the associated effects are analyzed in detail.

6. Future work

In the near future, the model will be integrated into the exiting system model and implemented on a RT system, which enables us to optimize a fuel cell powered system and design advanced controls. Further improvements are anticipated by taking into account the gas dynamics in the flow channel. At the same time, we plan to validate the models in a close collaboration with industry.

Acknowledgement

Yuyao Shan is grateful for the Fellowship from the Department of Mechanical Engineering at Auburn University.

References

[1] M. Ceraolo, C. Miulli, A. Pozio, J. Power Sources 113 (2003) 131–144.
[2] J.C. Amphlett, R.M. Baumert, R.F. Mann, B.A. Peppley, P.R. Roberge, T.J. Harris, J. Electrochem. Soc. 142 (1995) 9–15.
[3] S.D. Gurski, D.J. Nelson, et al., SAE 2003 World Congress and Exhibition, Detroit, 2003.
[4] Y. Zhang, M. Ouyang, Q. Lu, J. Luo, X. Li, Appl. Therm. Eng. 24 (2004) 501–513.
[5] P.R. Pathapati, X. Xue, J. Tang, Renew. Energy 30 (2005) 1–22.
[6] M. Wohr, K. Bolwin, W. Schnurnberger, M. Fischer, W. Neubrand, G. Eigenberger, Int. J. Hydrogen Energy 23 (3) (1998) 213–218.
[7] R. Eckl, W. Zehtner, C. Leu, U. Wagner, J. Power Sources 138 (2004) 137–144.
[8] J. Golbert, D.R. Lewin, J. Power Sources 135 (2004) 135–151.
[9] X. Xue, J. Tang, A. Smirnova, R. England, N. Sammes, J. Power Sources 133 (2004) 188–204.
[10] C. Maxoulis, Dimitrios, N. Tsnolou, G.C. Koltsakis, Energy Convers. Manage. 45 (2004) 559–573.
[11] H.M. Jung, W.Y. Lee, J.S. Park, C.S. Kim, Int. J. Hydrogen Energy 29 (2004) 945–954.
[12] http://www.emmeskay.com/fuelcell.pdf.
[13] B. Wetton, K. Promislow, A. Caglar, Second International Conference on Fuel Cell Science, Engineering and Technology, Fuel Cell, 2004.
[14] M. Sundaresan, Ph.D. Thesis, UC Davis, 2004.
[15] B. M. Eaton, Master Thesis, Virginia Technology, 2001.
[16] J.T. Pukrushpan, A. Stefanopoulou, H. Peng, Proceedings of the 2002 American Control Conference, 2002, pp. 3117–3122.
[17] M. Lampinen, M. Fomino, J. Electrochem. Soc. 140 (1993) 3537–3546.
[18] J.C. Amphlett, E.K. De Oliveira, R.F. Mann, P.R. Roberge, A. Rodrigues, J.P. Salvador, J. Power Sources 65 (1997) 173.
[19] Y.M. Ferng, Y.C. Tzang, B.S. Pei, C.C. Sun, A. Su, Int. J. Hydrogen Energy 29 (2004) 381–391.
[20] John P. Evans, Master Thesis, Virginia Technology, September 2003.
[21] http://webbook.nist.gov.
[22] P. Vie, S. Kjelstrup, Electrochim. Acta 49 (2004) 1069–1077.
[23] W. Yan, F. Chen, H. Wu, C. Soong, H. Chu, J. Power Sources 129 (2004) 127–137.
[24] T.E. Spriger, T.A. Zawodzinski, S. Gottesfeld, J. Electrochem. Soc. 138 (8) (1991) 2334–2342.